Green Chemistry

PAPER

View Article Online
View Journal | View Issue

Cite this: *Green Chem.*, 2025, **27**, 3964

Green catalyst-based cardboard waste conversion into biogas†

Li Quan Lee, ‡[a,b] Hui Ling Chan, ‡[c,d] Hao Zhou, [a,e] Hu Zhao, [a] Qingshuo Ao, [a] Hao Huang, [a] Chi Cheng Chong, [f] Yan Zhou [d] and Hong Li *[a,b]

Biofuels, such as biogas, are crucial for a sustainable and green energy future. Biogas can be generated from abundant biomass wastes, *e.g.*, corrugated cardboard waste (CBW), which has surged owing to e-commerce growth. Anaerobic digestion (AD) of CBW to generate biogas is challenged by the rate-limiting step of enzymatic hydrolysis and solid mass transport constraints. To address these issues, acid hydrolysis of carbohydrate components of CBW to a water-soluble sugar mixture is a more efficient alternative. Typical acid hydrolysis employs fossil fuel-derived sulphuric acid as the catalyst, which is unsustainable and may inhibit downstream bioprocesses. Herein, we report a novel mechanochemical-microwave pretreatment strategy that effectively overcomes the mass transport constraint of enzymatic hydrolysis. We replace the commonly used sulphuric acid with a renewable organic acid (*e.g.*, oxalic acid) as a green catalyst. Our new process with a green catalyst exhibits several advantages. The new mechanochemical treatment leveraging the catalytic effect during milling efficiently shrinks the CBW size, disintegrates its structure, and disperses the acid catalyst into CBW particles. The addition of oxalic acid facilitates dual-effect transformation of cellulose by reducing its degree of polymerization and converting crystalline cellulose into reactive amorphous cellulose through esterification of the C6–OH group, which disrupts intra- and intermolecular hydrogen bonds. Building on this, microwave-assisted hydrolysis further breaks down cellulose, where oxalic acid undergoes deprotonation to form hydronium ions, facilitating the cleavage of β-1,4 glycosidic bonds and releasing glucose products. This integrated process enhances overall efficiency and enables a much greener pretreatment. As a result, CBW's recalcitrant complex structure is effectively broken down, achieving a remarkable sugar yield of 52.3 g per 100 g dried CBW. The AD of the treated CBW, without additional separation steps, produced biogas with a high methane content of 69.9%, which is comparable to that of the control pure glucose feed. Notably, this whole-mixture approach significantly simplifies the process and boosts initial methane production without compromising long-term methane production potential. Moreover, life cycle assessment reveals that the process has a global warming potential comparable to that of traditional waste management processes, and the oxalic acid catalyst has a lower environmental impact than sulphuric acid, thus showing promise for enhanced sustainability.

Received 11th February 2025,
Accepted 7th March 2025

DOI: 10.1039/d5gc00740b

rsc.li/greenchem

Green foundation

1. This work introduces the replacement of fossil fuel-derived H_2SO_4 with the renewable, plant-derived organic acid catalyst oxalic acid (OA). Besides being greener, OA enables energy-efficient pretreatment of cardboard waste (CBW), reducing energy requirements in subsequent hydrolysis steps to address mass transport issues in anaerobic digestion (AD) feedstock and generating biogas without additional purification steps.
2. Our efficient method enables significantly faster sugar extraction, achieving the same yield approximately 18.5 times quicker than enzymatic hydrolysis. Our process offers substantial environmental benefits, demonstrating a 12.5% reduction in environmental impact through LCA by substituting H_2SO_4 with OA. This contributes to a much greener and more sustainable process. Additionally, our process exhibits a ~5-fold lower global warming potential (GWP) compared with landfilling.
3. The exploration of alternative biomass-derived organic acids could further enhance the environmental benefits and versatility of pretreating other wastes and downstream processes beyond AD.

[a]*School of Mechanical and Aerospace Engineering, Nanyang Technological University, Singapore. E-mail: ehongli@ntu.edu.sg*
[b]*CINTRA CNRS/NTU/THALES, UMI 3288, Research Techno Plaza, Nanyang Technological University, Singapore*
[c]*Conny Tech Pte Ltd, Singapore*
[d]*School of Civil and Environmental Engineering, Nanyang Technological University, Singapore*
[e]*Hubei Key Laboratory of Yangtze Catchment Environmental Aquatic Science, School of Environmental Studies, China University of Geosciences, Wuhan, Hubei, China*
[f]*School of Chemistry, Chemical Engineering and Biotechnology, Nanyang Technological University, Singapore*

† Electronic supplementary information (ESI) available. See DOI: https://doi.org/10.1039/d5gc00740b

‡ These authors contributed equally to this work.

1. Introduction

The depletion of fossil fuels and the increasing demand for alternative energy sources emphasize the importance of transitioning to sustainable options, such as low-carbon biofuels,[1] hydrogen fuel[2,3] and renewable energy.[1,4,5] Among the renewable energy sources, biofuels, such as methane-rich biogas, stand out as a reliable option for energy production owing to their stability under environmental fluctuations compared to solar or wind energy,[6,7] as well as them being an effective method for managing and utilizing waste materials. This is highly relevant for industries generating large amounts of waste, notably the surge in cardboard packaging consumption due to the rise of e-commerce and COVID-19 lockdowns, fuelled by China's online shopping growth (80% of 63.5 billion parcels in 2019).[8] Even in the garden city of Singapore, paper and cardboard waste (CBW) accounted for 15% of its municipal waste in 2022, amounting to 1.064 million tonnes.[9] Despite labor-intensive recycling efforts, only 37% of these materials are recycled owing to limitations and difficulties in separation and cleaning.[10–13] Alternatively, methods for managing cardboard waste also include incineration/landfill[14,15] and other applications, such as pyrolysis, to produce bio-oil and biochar,[16,17] building material fillers,[18,19] and bioethanol.[20] It is worth noting that incineration/landfill and pyrolysis are associated with inevitable carbon emissions/pollution issues. Building material fillers face many challenges in terms of weakened mechanical strength and poor long-term stability. Fermentation to bioethanol is very sensitive to contamination, which greatly impacts the ethanol yield. In contrast, the anaerobic digestion (AD) of untreated CBW to biogas[21–23] is a robust and environmentally friendly option, being less energy-intensive and cost-effective. CBW's suitability as a biogas feedstock stems from its reduced lignin and hemicellulose content and high cellulose content 59–75 wt%[24–26] resulting from the pulping process, making it more susceptible to sugar release.[25] The rigid and crystalline structure of cellulose in CBW, resulting from the intricate network of hydrogen bonds linking hydroxyl groups within and between chains,[27] is reinforced by the remaining lignin, hemicellulose, additives and adhesives (to give strength to corrugated cardboard).[28] This structure makes CBW challenging and time-consuming to break down during AD. The initial hydrolysis step of the AD process, which involves the enzymatic breakdown of complex organic molecules into simpler compounds by hydrolytic bacteria, is often the rate limiting step in many reactions.[29] Given the tougher structure of CBW, the process could take several days[30–34] to complete, depending on the feed composition and structure. Therefore, pretreatment processes, including physical,[35,36] biological[21] and thermochemical[37,38] methods, are essential to facilitate the hydrolysis process through the reduction of particle size and disruption of the reinforcement structure to increase cellulose accessibility.[39] Among them, acid hydrolysis is promising owing to its short duration, significantly reducing the overall process of biogas production.

Dilute acid hydrolysis of CBW also provides a more efficient alternative to enzymatic hydrolysis, depolymerizing cellulose and hemicellulose by cleaving the β-1,4 glycosidic bonds to release monomeric glucose and xylose. These water-soluble sugars, which are free from nondegradable lignin residue and mass transport limitation,[40] can then be readily converted by AD microbes to produce biogas.[41–43] For sugar extraction of lignocellulosic biomass, cost-effective inorganic acids (sulphuric, phosphoric, hydrochloric, and nitric acids) are often used,[44–48] which pose handling and logistical challenges owing to their corrosive and hazardous nature.[49] Furthermore, sulphuric acid can interfere with catalysts, inhibiting lignin graphitization,[50] and its toxicity could also impact downstream bioprocesses.[51] Most critically, these fossil-derived acid catalysts raise sustainability concerns and may become obsolete as the world transitions to renewable energy sources.[52] In contrast, organic acids derived from biomass, such as acetic, formic, and oxalic acids, offer a greener alternative as effective catalysts.[53] Notably, oxalic acid stands out owing to its strong acidity and excellent complexing ability.[54,55] Moreover, oxalic acid can be produced through microbial fermentation and is readily biodegradable, unlike sulfuric acid.[56] Previous studies have successfully utilized oxalic acid to extract sugars from oil palm waste,[57] corncob,[58] and other biomass,[59–61] primarily using hydrothermal methods.

Nevertheless, to the best of our knowledge, no study has introduced organic acid with a prior milling process to promote a mechanochemical reaction and further integrate it with microwave-assisted thermochemical hydrolysis. A few immediate advantages could emerge with such process integration. First, mechanochemical pretreatment offers a cost-effective, green alternative, leveraging mechanical force to

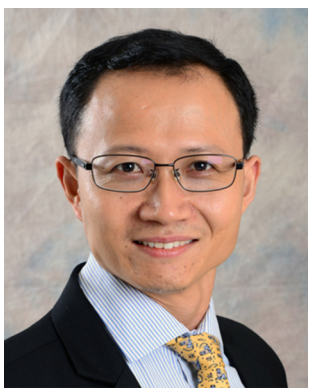

Hong Li

Dr Hong Li (Colin) received his bachelor degree and Ph.D. from Nanyang Technological University in Singapore. He was awarded the Singapore Millennium Foundation postdoctoral fellowship after graduation. In 2013, he joined the Mechanical Engineering Department at Stanford University as a postdoc, where he focused on electrocatalysis for green hydrogen generation (affiliated with the Center of Sustainable Energy through Catalysis). Dr Hong Li joined the School of Mechanical and Aerospace Engineering in June 2016 as Nanyang Assistant Professor, and he was promoted to Associate Professor with Tenure in March 2022. His current research interest includes biomass waste valorisation and green hydrogen, and he is leading a few

overcome diffusion barriers in solid–solid catalytic reactions, thereby enhancing cellulose depolymerization and reducing crystallinity.[62–66] Consequently, the following hydrolysis process is greatly enhanced by the waste feedstock with an enlarged surface area and porous/amorphous structure with a uniformly impregnated acid catalyst. Second, microwave-assisted thermochemical conversion boasts cost-effectiveness, rapid processing, and enhanced energy efficiency.[38,67–71] Our recent work on Paulownia wood valorization demonstrated the benefits of controlled microwave heating, achieving reduced reaction times, high selectivity, and enhanced sugar yields with minimal side products.[72] Finally, the organic catalyst, which replaces inorganic catalysts, greatly increases the sustainability of the process.

Herein, our study focuses on the use of solid oxalic acid as a sustainable and renewable chemical for processing CBW (see Fig. 1). Our innovative green acid mechanochemical-microwave pretreatment process involves two key steps: (i) ball-milling with OA, which transforms crystalline cellulose to amorphous cellulose *via* esterification of the C6–OH group, disrupting intra/inter-molecular hydrogen bonds; and (ii) microwave hydrolysis, where OA deprotonates to form hydronium ions, facilitating the cleavage of β-1,4 glycosidic bonds and releasing glucose products. This integrated process achieves an enhanced high glucose yield (~70%) in a single step, which has not been reported before. Furthermore, the process liquor can be directly converted into biogas with a high methane content of 69.9% through anaerobic digestion, achieving performance comparable to pure glucose feed. Additionally, a life cycle assessment (LCA) was conducted to evaluate the environmental benefits of the developed process and compare the environmental implications of oxalic and sulphuric acids. Overall, our efficient process transforms CBW into high-value products, such as glucose and renewable biomethane, to support a sustainable, low-carbon future.

2. Experimental section

2.1. Materials

Corrugated cardboard waste (CBW) was collected from used packaging boxes received through online shopping platforms. Chemicals from Sigma Aldrich included 5-hydroxymethylfurfural, acetic acid, ammonium formate, furfural, glucose, glycolic acid, levulinic acid, maleic acid, microcrystalline cellulose, oxalic acid, sulphuric acid (95%), tetrahydrofuran, and xylose. Methanol (LC/MS Grade) and ethanol were procured from Fisher Chemical and Aik Moh, respectively. The chemi-

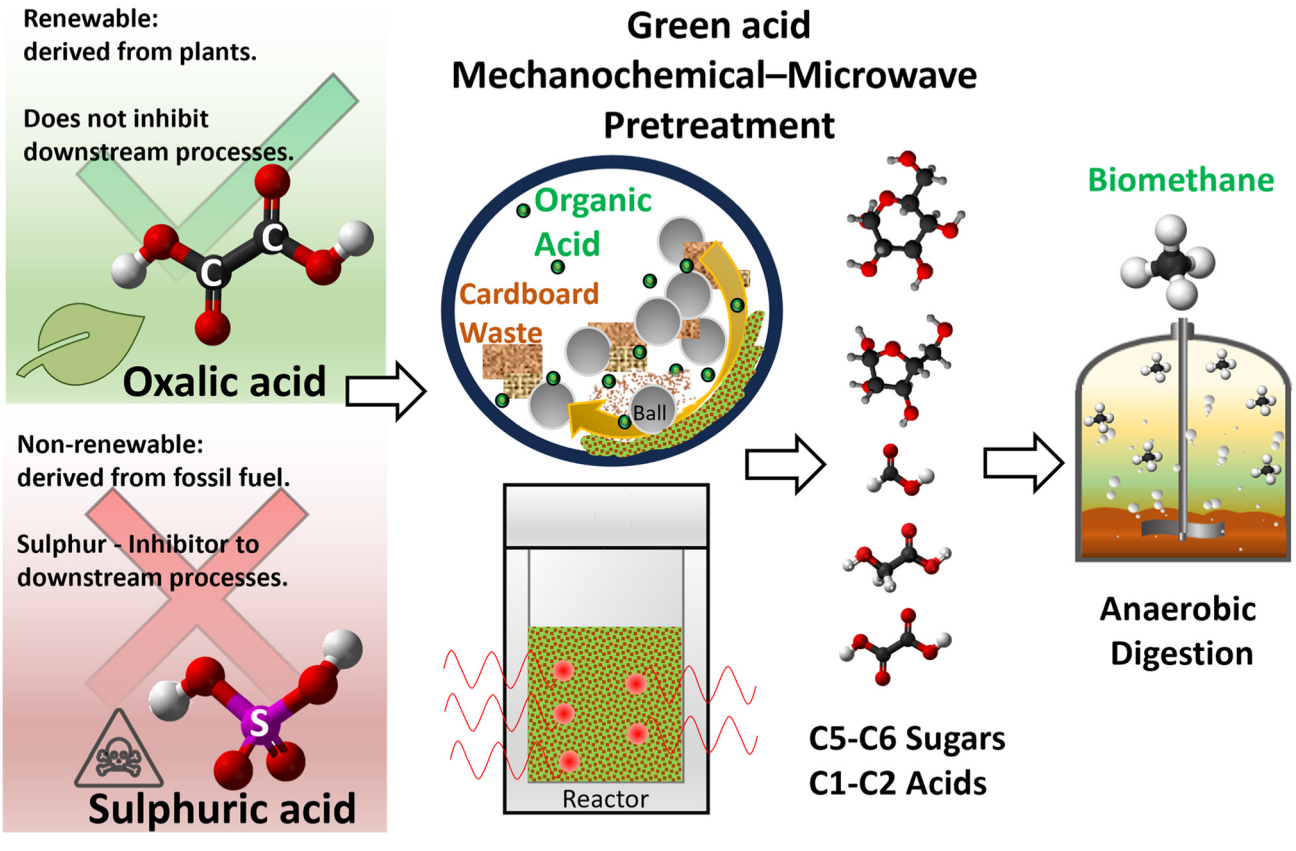

Fig. 1 Schematic of the greener route to valorise cardboard waste to biomethane: integration of oxalic acid-assisted mechanochemical and microwave processes to process cardboard waste to simple sugars and short-chain C1–C2 acids, followed by anaerobic digestion to methane.

cals were utilized as received, without purification. Ultra-pure water (Milli-Q-Millipore, resistivity of 18.2 MΩ cm) was utilized throughout this study.

2.2. Cardboard waste characterisation

Extractives were initially removed from the milled CBW using ethanol through a modified microwave-assisted extraction protocol.[73,74] Moisture, ash, and quantitative acid hydrolysis tests (NREL/TP-510-42618) were duplicated to determine lignocellulosic composition.[73,75,76] The CBW's average chemical composition is as follows: 8.4% ± 0.1% moisture, 1.1 ± 0.1% extractives, 55.5 ± 1.6% cellulose, 9.8 ± 1.9% hemicellulose, 15.9 ± 5.0% lignin and 10.0 ± 0.2% ash.

Surface, topographical, morphological, and compositional insights into CBW were obtained using scanning electron microscopy (SEM) on FESEM 700F, before and after pretreatment and MHT reaction. Samples were Au/Pd sputter-coated prior to analysis.

The particle size distribution of the milled CBW and cellulose samples was measured using a particle size analyser (Malvern, Mastersizer 2000) with a dispersion unit (Hydro2000 SM) stirred at 1000 rpm. Samples were dispersed in DI water to achieve an obscuration level of approximately 15%. The refractive indices were set as 1.560 (particle) and 1.330 (dispersant), with an absorption coefficient of 1. Triplicate measurements were taken, and the results were averaged and analyzed. The volume-weighted mean $D_{[4,3]}$ (V_w) was used to represent the average particle size of the samples.

X-ray diffraction (XRD) patterns were collected using a Shimadzu XRD-6000 diffractometer, enabling the examination of crystallinity and structural changes in cellulose within the CBW before and after pretreatment and the MHT reaction, with reference to the microcrystalline cellulose standard. Additionally, calcium carbonate, oxalic acid, and calcium oxalate (Whewellite) were characterized using X'Pert Highscore Plus software, referencing codes 00-005-0586, 96-724-1392, and 96-900-0764, respectively. The crystallinity index (CrI) of the samples was calculated using eqn (1):[77]

$$\mathrm{CrI}\,(\%) = \frac{I_c - I_{am}}{I_c} \times 100\%, \quad (1)$$

where I_c is the diffraction intensity for the crystal face (200) of cellulose at $2\theta = 22.7°$ and I_{am} represents the diffraction intensity of the amorphous cellulose domain at $2\theta = 18°$.

The degree of polymerization (DP) of cellulose from milled CBW was determined following a series of steps. First, cellulose was isolated from hemicellulose and lignin using an established method.[78] Then, the purified cellulose samples were then derivatized to cellulose tricarbanilate (CTC) for size exclusion chromatography (SEC) analysis, as described elsewhere.[79] 15 μL of dissolved CTC sample was injected during the SEC test, which provided the average molecular weight (Mw) used for the DP calculation. For SEC analysis, three Agilent PLgel 10 μm MiniMIX-B columns (250 × 4.6 mm) were connected in series using tetrahydrofuran as the mobile phase, flowing at 0.3 mL min^{-1} at 40 °C. The MiniMIX-B columns were operated within their specified range of 500–10 million (PS equivalents). The molecular weight obtained by converting from a universal calibration curve of polystyrene standards was used to calculate the CTC DP,[79] which was then calculated by dividing Mw by 519. This value was normalized to cellulose DP by multiplying by 1.5 to correct for a degree of substitution of 2.[80]

Fourier Transform Infrared (FTIR) spectroscopy with Attenuated Total Reflectance (ATR) was employed to identify the functional groups in the samples. The measurements were conducted using a Spectrum Two FTIR Spectrometer equipped with a diamond ATR crystal. After being washed and dried, the samples were firmly pressed against the crystal using a pressure clamp to ensure good contact. Spectra were recorded in the wavenumber ranging from 4000 to 400 cm^{-1} with a spectral resolution of 4 cm^{-1}. Each spectrum was averaged over 10 scans to improve the signal-to-noise ratio. A background spectrum was acquired before each sample measurement to correct for ambient atmospheric conditions. Data processing, including baseline correction and normalization, was performed using the spectrum IR software. The main infrared peaks identified in the FTIR spectra of the CBW samples, corresponding to specific molecular vibrations, are reported in Table S1.†

2.3. Pretreatment of cardboard waste

Following simple cleaning, the CBW was cut into approximately 4 mm × 4 mm square pieces (Fig. S1a†). The CBW (2.5 g) was then milled in a ball milling apparatus (Retsch, E-max) with 153 g of 5 mm ZrO_2 balls in a 125 mL ZrO_2 jar (Fig. S1b†). Oxalic acid (OA) was added during milling at varying weight percentages: 10.1, 18.4, 31.0, and 47.4 wt% (based on the ratio of OA weight to the total weight of OA and CBW). After milling, 50 mL of DI water was pipetted into the funnel cover of the self-made sieve-vortex device (Fig. S1c†) to separate the milled CBW from the milling balls. This step diluted the previously added OA to final concentrations of 0.53, 1.06, 2.10, and 4.11 wt% OA. The resulting pretreated slurry was collected directly into a centrifuge tube with minimal loss of materials, which ensured accurate mixture preparation.

The OA-CBW slurry samples were hydrothermally reacted in a microwave reactor (Anton Paar, Multiwave 5000) using a 50 mL reactor vessel with a solid-to-liquid loading of 0.75 g to 15 mL. The reaction conditions included varying maximum temperatures (140, 160, or 180 °C) at a fixed ramp rate (0.29 °C s^{-1}) of fixed reaction time (5–60 min). The vessel was then cooled to 45 °C internally, after which the supernatant was centrifuged, extracted, and refrigerated at 4 °C for subsequent product analysis.

Liquid product samples from microwave hydrothermal treatment were adjusted to pH 6–7 and filtered through 0.45 μm syringe filters before analysis using an Agilent 1200

HPLC system. For sugar and organic acid quantification, an Agilent Hi-Plex H column (7.7 × 300 mm, 8 μm) was employed with refractive index detection using 0.01 M sulphuric acid as the mobile phase at 0.6 mL min^{-1}. Sugar separation and the corresponding calibration curves are shown in Fig. S2 and S3,† respectively, which demonstrate the effective separation and quantification of sugars in our HPLC method. The injection volume was 20 μL, with a 25 minute run time at 50 °C. Furfural and 5-HMF concentrations were determined using an InfinityLab Poroshell 120 Aq-C18 column (4.6 × 150 mm, 2.7 μm) with multi-wavelength detection (220 nm). The mobile phase consisted of methanol and 5 mM ammonium formate (3 : 7, v/v) at 0.6 mL min^{-1}, with a 20 μL injection volume and a 10 minute run time at 40 °C.

The measured sugar concentration and initial sugar content from the chemical composition analysis of CBW were used to determine the sugar yield % as follows:

$$\text{Sugar yield}\,(\%) = \frac{\text{Mass of sugar product}}{\text{Mass of potential sugar product in substrate}} \times 100\%, \quad (2)$$

where sugar is glucose or xylose, and substrate is CBW or cellulose.

The total sugar yield based on 100 g of dried CBW was calculated using eqn (3):

$$\text{Sugar yield}\,(\text{g per 100 g of dried CBW}) = \frac{\left(\text{concentration of xylose}\,(\text{g l}^{-1}) + \text{concentration of glucose}\,(\text{g l}^{-1})\right) \times \text{volume of hydrolysate}\,(\text{l})}{\text{Mass of dried CBW}\,(\text{g})} \times 100\%. \quad (3)$$

Total organic carbon (TOC) and inorganic carbon (IC) in both the solid and liquid phases were analyzed using a Shimadzu TOC 5000A analyzer.

For NMR analysis, the samples were lyophilized and reconstituted in D_2O. A 0.7 mL aliquot was transferred to an NMR tube, and ^1H NMR spectra were recorded using a JEOL ECA400 spectrometer at 400 MHz at room temperature.

Gel Permeation Chromatography (GPC) analysis was conducted using an Agilent 1260 Infinity Multi-detector GPC/SEC system with a refractive index detector. A series-coupled column setup consisting of Agilent PL aquagel-OH 20, 40, and 60 columns (8 μm, 7.5 × 300 mm each) was employed to determine the molecular weight of various samples. Before analysis, samples (1–2 mg mL^{-1}) were adjusted to pH 9 with KOH, filtered through 0.2 μm filters, and then injected (100 μL) into the system. Elution occurred with HPLC-grade water at 0.7 mL min^{-1}. The column oven and RI detector were maintained at 35 °C. Calibration was performed using PEG/PEO standards (Agilent Easivial) spanning a molecular weight range of 194–1 250 000 Da, generating an 11-point calibration curve.

After optimization of the hydrothermal parameters to achieve the highest sugar yield, the hydrolysate of cardboard in oxalic acid (CBW-OA) was used in subsequent anaerobic digestion.

2.4. Anaerobic digestion of pretreated cardboard waste

The batch experiments were conducted at 35 °C in 0.5 L glass bottles in duplicates. The bottles were filled with 0.4 L of laboratory-maintained sludge inoculum, characterized by a total suspended solid (TSS) concentration of 17.2 g L^{-1} and a volatile suspended solid (VSS) to TSS ratio of 0.6. TSS and VSS were determined according to standard methods 2540B and 2540E, respectively (APHA, 2012). The bottles were then sealed, and the headspace was flushed with pure nitrogen (N_2) for 5 min, before connecting the bottle to a gas bag. The experiment took place in an incubator shaker (ZQZY-75AN, Shanghai Zhichu Instrument, China) set to 150 rpm.

At the start of the experiment, glucose and CBW-OA feedstock (851 ± 23 mg COD), equivalent to approximately 1217 mg of dried CBW, were added to duplicate reactor bottles to monitor CH_4 production. Glucose was used as a substrate for the baseline comparison as a preferred carbon source,[81] allowing efficient uptake and conversion to methane in typical anaerobic digestion systems and avoiding complications, such as toxicity and kinetic delay, from more complex biomass sources. Biogas production was quantified by measuring the volume of the gas bag at regular intervals over a fixed duration. The test was terminated when the gas production decreased to approximately 1% of the accumulated gas volume, corresponding to a 10 day test duration for both feedstocks.[82]

The soluble fraction of centrifuged (8500 rpm, 30 min) and filtered (0.22 μm nylon syringe filter) sludge samples were analyzed weekly for volatile fatty acid (VFA) composition (C2–C7) using an Agilent 8890B GC-FID with a DB-FFAP column (30 m). The GC conditions were 0.5 μL injection volume, nitrogen carrier gas, 16 min runtime, and 205 °C.

Biogas composition was analyzed using an Agilent 7890A GC with double thermal conductivity detectors and multiple columns (MolSieve 13×, MolSieve 5 Å, and HaySep C, 3 m each). The GC conditions included helium and nitrogen carrier gases at 220 °C. Peak areas for H_2, CO_2, CH_4, and N_2 were identified and quantified against individual gas calibration curves to determine the percent composition.

2.5. Life cycle assessment

According to ISO 14040 and ISO 14044,[83,84] the main steps of LCA in this study are (1) definition of the goal and scope, (2) collection of data and preparation of life cycle inventories (LCI), (3) selection of life cycle impact assessment (LCIA) methods, and (4) interpretation of life cycle impact assessment results.

2.5.1. Goals, scope, and the evaluated scenarios of this study. The functional unit (FU) used in this study treats 100 kg of CBW based on lab-scale experiments. The chemical composition values of CBW are listed in Table S2.† The system boundary of each treatment scenario begins with the collected CBW and ends with the disposal or use of the final products (Fig. S4†).

2.5.2. Life cycle inventory analysis and data acquisition. The LCI foreground data in this study were mainly sourced from the experimental results, the published studies, and related calculations based on the mass balance. The detailed inventories of all treatment scenarios are shown in Tables S3–S6.† Background inventory data, including electricity, chemicals, and materials, were obtained from the Ecoinvent 3.5 database, as listed in Table S7.† It is noteworthy that the background inventory data for oxalic acid production are derived from the literature (Table S8†).

2.5.3. LCIA was conducted using SimaPro v9.1 software. Eighteen environmental impact categories in the ReCiPe 2016 midpoint method were used to evaluate environmental performance. These eighteen indicators were grouped into five categories based on their relevance to air, water, soil, human health, and resource depletion. The air-related categories include global warming potential (GWP), particulate matter formation potential (PMFP), ozone formation potential ecosystems (EOFP), and ozone depletion potential (ODP). Water-related categories include freshwater eutrophication potential (FEP), marine eutrophication potential (MEP), freshwater ecotoxicity potential (FETP), marine ecotoxicity potential (METP), and water consumption potential (WCP). The soil-related categories include terrestrial acidification potential (TAP), terrestrial ecotoxicity potential (TETP), and land use (LU). Human health-related categories include human carcinogenic toxicity potential (HCTP), human non-carcinogenic toxicity potential (HNCTP), ionizing radiation (IR), and ozone formation potential human health (HOFP). The resource depletion-related categories include mineral depletion potential (MDP) and fossil depletion potential (FDP). Moreover, the total normalized environmental impact values (dimensionless) were obtained by weighting and summing each environmental impact category using the normalization factors in the "World (2010) H" (Table S9†).

3. Results and discussion

3.1. Mechanochemical pretreatment of cardboard waste

To optimize the ball milling conditions for our cardboard waste (CBW) studies, we systematically varied the rotation speeds and milling times. Milling at 1000 rpm for 30 minutes yields optimal particle sizes, with up to 90 wt% of particles below 400 μm. Notably, further size reduction beyond this point does not significantly enhance sugar yield during biomass hydrolysis, making this condition ideal for subsequent processing steps.[85] This optimized milling condition was used for all subsequent experiments, including the control sample and those involving co-milling. The SEM image of the control sample in Fig. S5a† exhibits the characteristic fibrous structure of cardboard, comprising cellulose fibers.

As shown in Fig. 2a and Fig. S5b,† the higher-magnified SEM images display fragmented particles with smooth surfaces, indicating effective milling and increased surface area. In contrast, after CBW was co-milled with OA, the fibrous characteristic of the cardboard was no longer evident, as shown in the SEM image (Fig. S5c†), where smaller particles appeared as broken bits and pieces. This indicates an extensive breakdown of the lignocellulosic structure during co-milling. Furthermore, the SEM images (Fig. 2b and Fig. S5d†) exhibit an apparent increase in surface roughness and porosity. The CBW particles display a porous structure with numerous small pores (~0.1 μm), indicating enhanced reactivity and accessibility for subsequent acid hydrolysis. These changes can be attributed to the combination of mechanical energy and hot spots generated during ball milling,[86] which could activate the potential chemical etching effect of OA. This inevitably leads to the breakdown of starch-based adhesives commonly used in corrugated cardboard production and potentially decreases CBW cellulose's degree of polymerization and crystallinity, which is essential to increase sugar yield output in subsequent processes.[87]

Fig. 2c illustrates the impact of increasing OA concentration on the CBW particle size distribution. Adding 18.4 wt% OA reduces the average particle size by 30% compared to the control sample. However, a residual hump remains at the tail of the distribution, indicating that OA is insufficient to fully impact larger particles. Indeed, increasing the OA concentration to 31.0 wt% eliminates the remaining larger particles, resulting in a narrower particle size distribution. The mean particle size decreases as the OA concentration increases with a maximum reduction of 58.5% when 47.4 wt% OA was added, resulting in a clear shift towards smaller particle sizes. A similar 52% size reduction was observed when microcrystalline cellulose was co-milled with OA (Fig. S6a†). This suggests that OA acts as a grinding aid, improving pulverization efficiency similar to grinding auxiliaries used in various industries.[88,89]

To investigate the effects of co-milling with OA and MHT treatment on the crystalline structure of cellulose, the primary component of CBW, XRD patterns were examined (Fig. 2d). The cellulose standard exhibits characteristic peaks at 15°, 22.5°, and 35°,[90] which are also present in the CBW-control sample, confirming the presence of crystalline cellulose. Additionally, peaks corresponding to calcium carbonate (commonly used as fillers for cardboard)[91] are detected in the CBW-control sample. In contrast, after co-milling with OA, the typical XRD peaks of crystalline cellulose (15° and 35°) are absent, indicating the transformation of crystalline cellulose to an amorphous form. The XRD patterns also reveal the presence of the OA catalyst, confirming successful impregnation into CBW. Notably, after the microwave treatment, the remaining solid sample (post MHT co-milled OA) exhibits a drastically different peak pattern, which is attributed to calcium

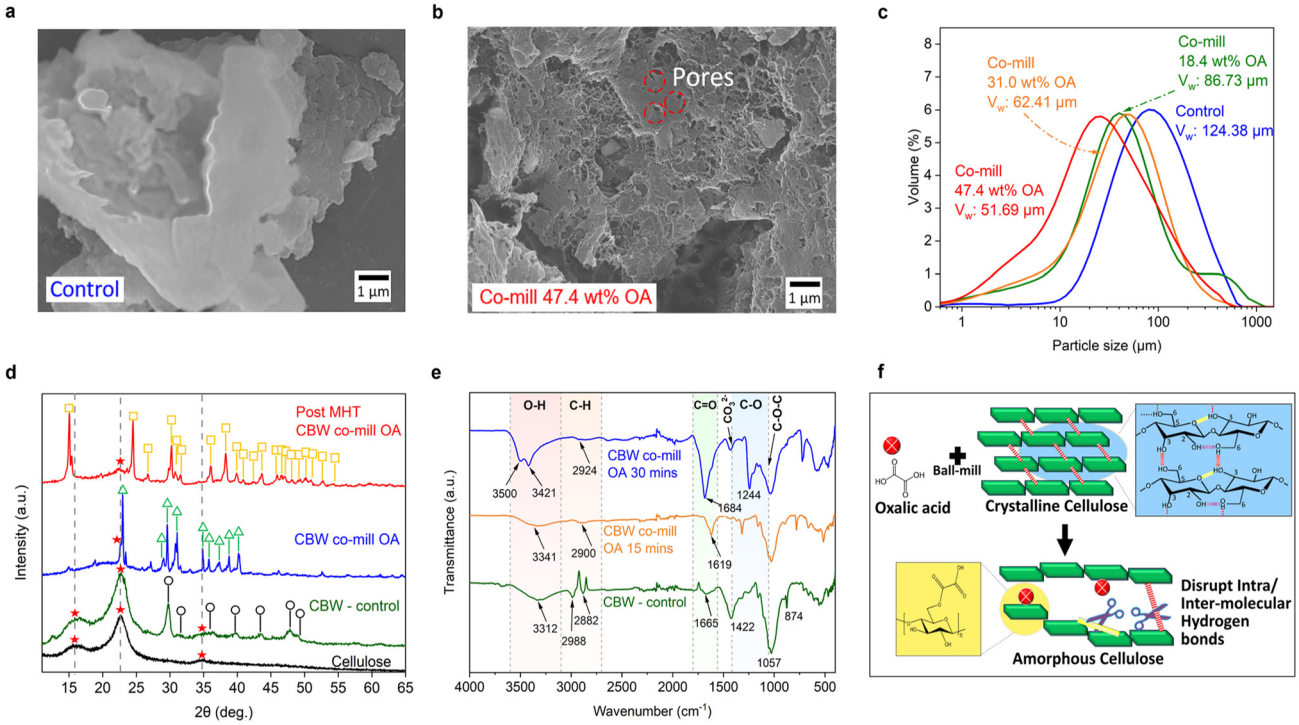

Fig. 2 Oxalic acid mechanochemical treatment on cardboard waste (CBW). FE-SEM images of CBW samples: (a) control (milled without the catalyst), (b) co-milled with 47.4 wt% oxalic acid. (c) Influence of varying solid oxalic acid amounts on cardboard particle size distribution. XRD patterns of (d) the cellulose standard (black), CBW control sample (green), CBW co-milled with 47.4 wt% oxalic acid (blue), and post-microwave hydrothermal treatment of CBW co-milled with oxalic acid (red). Peak labels: red star = cellulose peaks, black circle = calcium carbonate, green triangle = oxalic acid and yellow square = calcium oxalate. (e) FTIR spectra of CBW control and co-milled with oxalic acid at different duration. (f) Schematic of oxalic acid-mediated cellulose transformation during co-milling, illustrating the disruption of hydrogen bonds (intramolecular: purple and yellow stripes; intermolecular: red stripes).

oxalate formation ($CaCO_3 + H_2C_2O_4 \rightarrow CaC_2O_4 + H_2O + CO_2$), a byproduct of OA reaction with calcium carbonate.[92] These findings suggest that co-milling with OA and subsequent MHT treatment can effectively disrupt cellulose crystallinity and hydrolyse cellulose to soluble oligo/monosaccharides, respectively.

The decrease in DP was further substantiated by Size Exclusion Chromatography (SEC) analysis of the control and co-milled OA samples. As presented in Table S10,† optimal basic ball milling reduced the DP of cellulose in CBW to 422, which is significantly lower than the DP value of 1635 reported in another study, where chemical treatment reduced the DP to 485.[93] Notably, co-milling with OA led to a drastic reduction in DP by as much as 4 times, resulting in a DP of 102. The decrease in DP directly correlates with an increase in reducing ends, as shorter cellulose chains have more terminal glucose units with free aldehyde groups, thus enhancing cellulose reactivity.

FTIR spectra (Fig. 2e) reveal the transformation of cellulose from crystalline to amorphous in CBW with OA over increasing milling time, as evidenced by hydrogen bonding changes in the O–H stretching region (3100–3600 cm^{-1}). Notably, the peak shift to higher wavenumbers in the O–H region indicates the amorphous transformation of the cellulose structure, which may be caused by the scission of intra- and intermolecular hydrogen bonds. The calculated hydrogen bond energy and asymmetric index (Fig. S7a†) suggest reductions in hydrogen bonding and crystallinity, respectively.[94] The amorphous nature of the cellulose is further verified by the increased shift and diminished intensity of the C–H stretching vibration band, from 2882 cm^{-1} to 2924 cm^{-1}. The disappearance of the peak (2988 cm^{-1}) after OA treatment during ball milling may be attributed to the degradation of lignocellulosic methyl groups, leading to an increasingly rougher surface and pore formation, consistent with the SEM images (Fig. S8†). The O–H, COOH and C–O peaks at 3500 cm^{-1}, 1684 cm^{-1} and 1244 cm^{-1}, respectively, are assigned to OA, indicating its impregnation into the CBW after 30 min of ball-milling. Owing to peak overlap at 1684 cm^{-1}, curve fitting analysis was performed (Fig. S7b†), revealing carboxylate peaks at 1687 cm^{-1}, 1642 cm^{-1}, and the ester peak at 1747 cm^{-1}.

The proposed mechanism (Fig. 2f) illustrates the transformation of crystalline cellulose to amorphous cellulose *via* esterification of the C6–OH group upon the addition of OA to CBW during ball milling. Consequently, these charged acid groups may disrupt the intra/inter-molecular hydrogen bonds,[95] leading to the amorphous form. This is consistent with the XRD patterns in Fig. S9a,† highlighting the optimal acid co-milling duration of 30 min, which drastically reduced the crystallinity of cellulose in CBW (Fig. S9b†).

Our results demonstrate that co-milling cardboard waste (CBW) with OA offers several benefits, including enhanced OA dispersion in CBW, significant reductions in particle size and DP, and increased surface area and porosity. Essentially, this process transforms crystalline cellulose into reactive amorphous cellulose, which is more easily hydrolyzed,[96] leading to more efficient biomass processing.

3.2. Microwave pretreatment of cardboard waste to sugar

Microwave hydrothermal treatment (MHT) enhances acid hydrolysis, which is a crucial step in extracting sugars from CBW. To evaluate the effectiveness of this process, we investigate the effect of microwave pretreatment on CBW with OA and compare its performance with other acid catalysts, namely sulfuric acid, acetic acid (HAc), and tartaric acid (TA), under the same MHT conditions. OA outperformed the other organic carboxylic acids, which can be attributed to its stronger acid strength, characterized by pK_a values of 1.23 and 4.26 for the first and second proton dissociations, respectively.[97,98] This resulted in the highest sugar yield (Fig. S10a†) and fewer degraded sugar products (Fig. S10b†). Stronger acids are expected to release more sugars owing to their higher H^+ ion concentrations, where H^+ ions initiate cellulose hydrolysis by attacking the β-1,4-glycosidic bond. Owing to its strong oxidizing and acid strength properties and a diprotic acid (a proton is more likely donated to the solvent), sulfuric acid exhibited severe reactions, resulting in a significantly lower sugar yield. This is attributed to the dehydration of hydrolyzed sugars, where xylose was converted to furfural and glucose dehydration formed 5-HMF, which was further hydrated to produce levulinic acid.[99]

To further elucidate the impact of OA co-milled on cellulose conversion efficiency during MHT, we conducted a preliminary study using microcrystalline cellulose (MCC). Co-milled MCC with OA significantly enhanced the sugar yield, resulting in a 5.5-fold increase compared to MCC milled without OA (control) after just 5 min of MHT (Fig. S6b†), which is attributed to the transformation of cellulose to its amorphous form. This improvement also correlates with the reduced particle size and increased surface area of OA-co-milled MCC, facilitating more efficient cellulose accessibility and conversion to glucose.

Motivated by these findings, we systematically optimized the microwave pretreatment conditions to maximize the total sugar yield. First, we varied acid concentrations at a fixed temperature of 180 °C for 30 min. Then, using the optimized acid concentration, we explored the temperature and duration combinations to further enhance the sugar yield. Fig. 3a com-

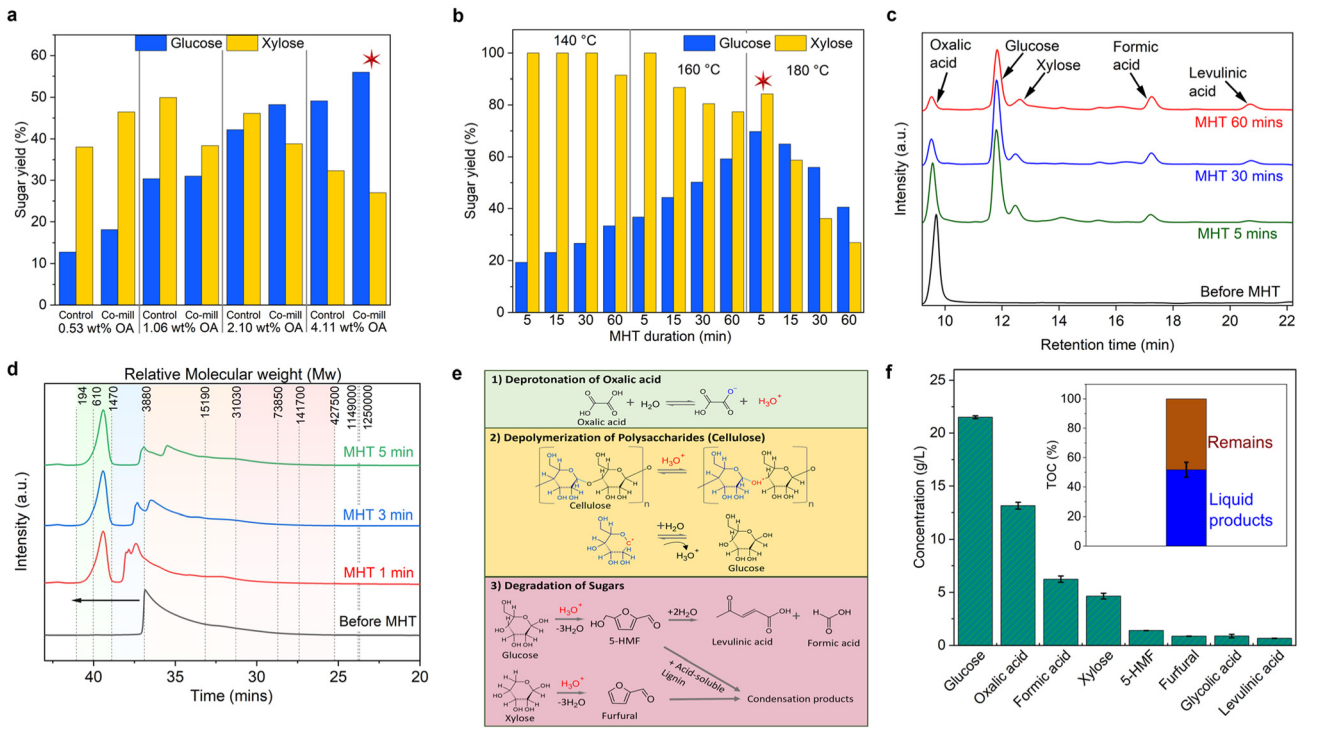

Fig. 3 Optimization of microwave hydrothermal treatment parameters for maximum total sugar yields from CBW: (a) effect of oxalic acid catalyst concentration co-milled with CBW on xylose and glucose yield in the microwave-assisted hydrothermal process at 180 °C for 30 min compared with control milled samples. (b) Effect of MHT temperature and time on xylose and glucose yields using 4.11 wt% OA co-mill CBW. (c) HPLC chromatograms showing product formation over time. (d) GPC chromatograms of liquid products before and after MHT of CBW-OA at varying duration. (e) Schematic of oxalic acid hydrolysis of polysaccharides in CBW to sugars and further sugar degradation to other products. (f) Quantification of liquid products and inset: TOC analysis for carbon balance estimation. Note: Liquid TOC values were corrected for added oxalic acid and formic acid. *Red stars denote the parameters for achieving the optimal sugar yield.

pares the sugar yield after microwave hydrothermal treatment (MHT) of CBW using different OA concentrations with and without co-milling. Notably, all the CBW samples with co-milling showed a significant increase in glucose yield. However, high OA concentrations (>0.53 wt%) led to decreased xylose yield owing to side dehydration reactions. The highest total sugar (glucose + xylose) yield was achieved after the MHT of the co-milled CBW (4.11 wt% OA), as shown in Fig. S11a.† The formation of smaller organic by-products (Fig. S11b†) followed an expected increasing trend with higher OA concentrations. Formic acid was detected from partial OA decomposition, while levulinic acid, lactic acid, acetic acid, and glycolic acid were present in minimal amounts, less than 5 g per 100 g dried CWB, highlighting the low by-product yield when using OA as an organic acid catalyst.

Fig. 3b demonstrates further optimization of the MHT process with a fixed OA concentration (4.11 wt%). Notably, at 140 °C, a 100% xylose yield was achieved in just 5 min with a 20% glucose yield. Increasing the temperature to 160 °C enhanced the glucose yield to 36.7%, as increased input thermal energy accelerates hydrolysis kinetics. The maximum glucose yield (69.8%) was achieved at 180 °C in only 5 minutes but decreased with prolonged MHT duration owing to glucose dehydration.

HPLC analysis (Fig. 3c) confirms the time-dependent changes in compound concentrations, elucidating the aforementioned reaction mechanism. Microwave treatment initially promotes polysaccharide hydrolysis to glucose and xylose, leading to a significant increase in total sugar yield within the first 5 min. As treatment time progresses, glucose further degrades to levulinic acid, causing a decline in glucose yield and a corresponding increase in levulinic acid production. Concurrently, OA decomposes to formic acid,[100] as evidenced by the reduction in OA and the elevated formic acid levels. Furthermore, the decline in OA levels may be attributed to the formation of insoluble calcium oxalate, as previously indicated by the XRD analysis.

GPC chromatograms (Fig. 3d) further provide insight into the molecular evolution of the OA co-milled products before and after MHT, as a function of treatment duration. The molecular weight distribution is categorized into four ranges (Fig. S12†) to facilitate quantification and elucidate the underlying mechanisms of the MHT process. Notably, within the first minute of the reaction, a significant reduction in molecular weight is observed, accompanied by the formation of intermediates from polysaccharide depolymerization into oligomers and monomers. As the reaction proceeds, a gradual increase in larger molecular weight distributions emerges, which is likely attributed to the condensation of sugar by-products and lignin fragments.[101]

Using the HPLC and GPC analysis results, we propose a mechanism (Fig. 3e) involving three key steps. First, oxalic acid deprotonates to form hydronium ions (H_3O^+) in the presence of water. Subsequently, MHT facilitates the attack of H_3O^+ on the β-1,4 glycosidic oxygen bond of cellulose. The positive charge is then transferred to the C1 position, resulting in the formation of a cyclic carbonium ion and the subsequent cleavage of the glycosidic bond. This is followed by a rapid attack by a water molecule on the carbonium ion, releasing a free glucose residue and regenerating the proton.[102] Finally, the released glucose and xylose undergo further degradation through a series of reactions, including dehydration, isomerization, and rehydration, yielding compounds such as furfural and 5-HMF. Owing to the severity of the treatment increases, these products may undergo condensation reactions with acid-soluble lignin to form high molecular weight products, such as pseudo-lignin polymer and humin.[103]

Under optimized conditions (180 °C, 5 min, 4.11 wt% OA), the hydrolysate (CBW-OA) achieves a remarkable sugar yield, producing 21.5 g L^{-1} glucose and 4.6 g L^{-1} xylose, with minimal sugar degradation products of less than 2 g L^{-1} (Fig. 3f). This is consistent with the ^{1}H NMR spectrum (Fig. S13a†), displaying peaks at 3–4 ppm indicative of glucose and xylose sugars,[104] as well as signals for formic acid and a trace amount of acetic acid. The inset TOC analysis image shows a 50% dissolution, releasing half of CBW's organic carbon, with glucose being the dominant TOC product (Fig. S13b†). The remaining fraction likely comprises lignin and unreacted cellulose, and calcium oxalate exhibits a significant reduction in particle size and increased porosity after MHT, as observed by SEM (Fig. S5e†). High-magnification imaging (Fig. S5f†) reveals composite material agglomeration of nanospheres, which could be utilized for developing sustainable 'green concrete' building materials.[105,106]

Overall, our mechanochemical-microwave pretreatment of CBW achieves a remarkable total sugar yield of 52.32 g per 100 g dried CBW, which is the highest among other dilute acid hydrolysis studies on various lignocellulose feedstocks, as presented in Table S11.† Our efficient method also enables sugar extraction approximately 18.5 times faster than enzymatic hydrolysis, achieving the same sugar yield,[33] which paves the way for more sustainable and cost-effective biofuel production.

3.3. Anaerobic digestion of pretreated Cardboard waste

Following the optimized microwave pretreatment of CBW, the processed feed (CBW-OA) was subjected to anaerobic digestion to evaluate its potential for methane production. As shown earlier in our analysis, the pretreated CBW-OA feed consists of digestible organic carbons from a mixture of small organic acids and sugars, including glucose, xylose and OA, as well as a low amount of furfural and 5-HMF that could be potentially toxic and inhibitory to microbial communities.[107] We then compared the biomethane yield of CBW-OA to that of pure glucose, a widely used control feed in biogas production.[43,81,108] As shown in Fig. 4a, the CH_4 content in the biogas from pretreated CBW feed is higher than the glucose feed, especially during the initial gas production phase (day 0–7), peaking at 69.9% on day 7. This could be attributed to

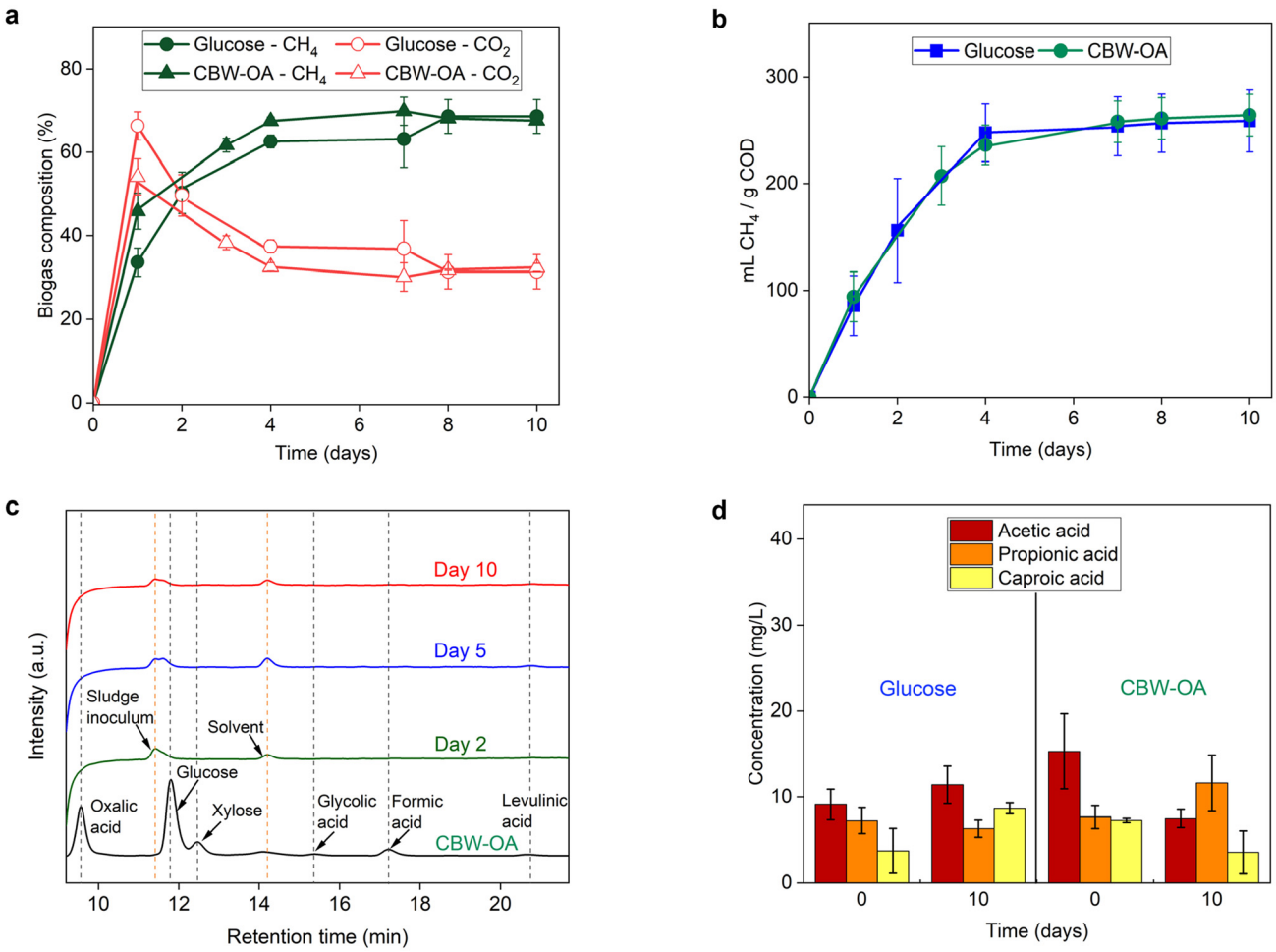

Fig. 4 Methane production from cardboard waste (CBW) feed *via* anaerobic digestion over 10 days. Comparison of CBW-OA feed *vs*. glucose control with (a) biogas composition, and (b) cumulative methane production. (c) HPLC chromatogram: consumption of organic acids and sugars in CBW-OA feed. (d) Concentration of volatile fatty acids in CBW-OA and glucose feed.

the presence of shorter carbon chain products (C1 and C2) in the CBW, such as formic acid and OA, which can be quickly broken down into viable substrates for immediate methane production. Formic acid can also be directly consumed by methanogens to produce CH_4.[109] This reduces the intermediary steps typically required for the breakdown of longer-chained products, which otherwise leads to increased CO_2 production.

The cumulative methane yield from glucose and CBW-OA substrates (Fig. 4b) increased rapidly from day 1 to 4, during which 96% of the cumulative methane production was observed for glucose and 89% for CBW-OA. The cumulative methane yield increased slowly thereafter and converged for both substrates, with CBW-OA observing a slightly higher cumulative methane production (2%) than glucose at day 10. The final methane yield for CBW-OA is 264 mL CH_4 per g COD, which is equivalent to 122 mg CH_4 per 1000 mg of dried CBW and is comparable to pure glucose for long-term methane production potential.

The HPLC analysis (Fig. 4c) substantiates the rapid consumption and breakdown of the organics in the AD, as the initial products were no longer detected from day 2 onwards. This demonstrates the effectiveness of the pretreatment in overcoming the main limitation of methane production, namely the low hydrolysis rate caused by the complex and compact structure of lignocellulosic biomass.[110]

Quantification of VFA (Fig. 4d) shows similar trace amounts of VFA for CBW OA and glucose feed (<20 mg L^{-1}) at the start and the end of each experiment, indicating that all feed CODs were consumed at the end of the experiment.

In summary, our study demonstrates that microwave-pretreated CBW-OA, used as a whole mixture without glucose separation or extraction, exhibits enhanced biomethane production potential comparable to glucose feed while simplifying the process and reducing energy requirements. The presence of shorter carbon chain products in the feed boosts the initial methane content without compromising the robust long-term methane production potential. These findings suggest that microwave-pretreated CBW-OA is a promising

feedstock for anaerobic digestion and for future biogas upgrading to biomethane.

3.4. Life cycle assessment

The environmental impacts generated from the various CBW treatment routes were analysed by LCIA, with a focus on the global warming potential (GWP) of the processes in terms of equivalent CO_2 emission. The GWP impact was assessed based on seven different scenarios, including five ways to provide electricity to our CBW process and two conventional waste treatment processes, as depicted in Fig. 5a. When CBW is processed by the mechano-bio-thermochemical (MBTC) method, the major GWP contributors are electricity generation for the hydrolysis process, carbon emission from the combined heat and power (CHP) system, followed by OA production. The GWP arising from electricity generation can be reduced by 95% when the source is switched from natural gas/fossil fuel to renewable solar or wind energy, except for hydroelectricity. Notably, in the conventional treatment of CBW, *viz.*, the landfill has the highest GWP with the uncontrolled release of methane gas to the environment. Our MBTC process, when coupled with renewable energy sources, has a much lower global warming potential than landfills. However, it is slightly higher than the conventional incineration process. This is due to the release of greenhouse gases in the environment when the biogas generated from AD was combusted in the CHP system.

Fig. 5b shows a breakdown of the GWP contribution by various process components in the CBW MBTC system when it is powered by photovoltaics. The major GWP contributor is from the CHP system as aforementioned. In contrast, ball milling, hydrolysis, filtration and AD when driven by solar power provide large carbon savings compared to fossil fuel (*e.g.*, natural gas)-based electricity. Other auxiliary processes, such as water and waste treatment, contribute relatively little to the GWP of our process. Notably, our process when driven

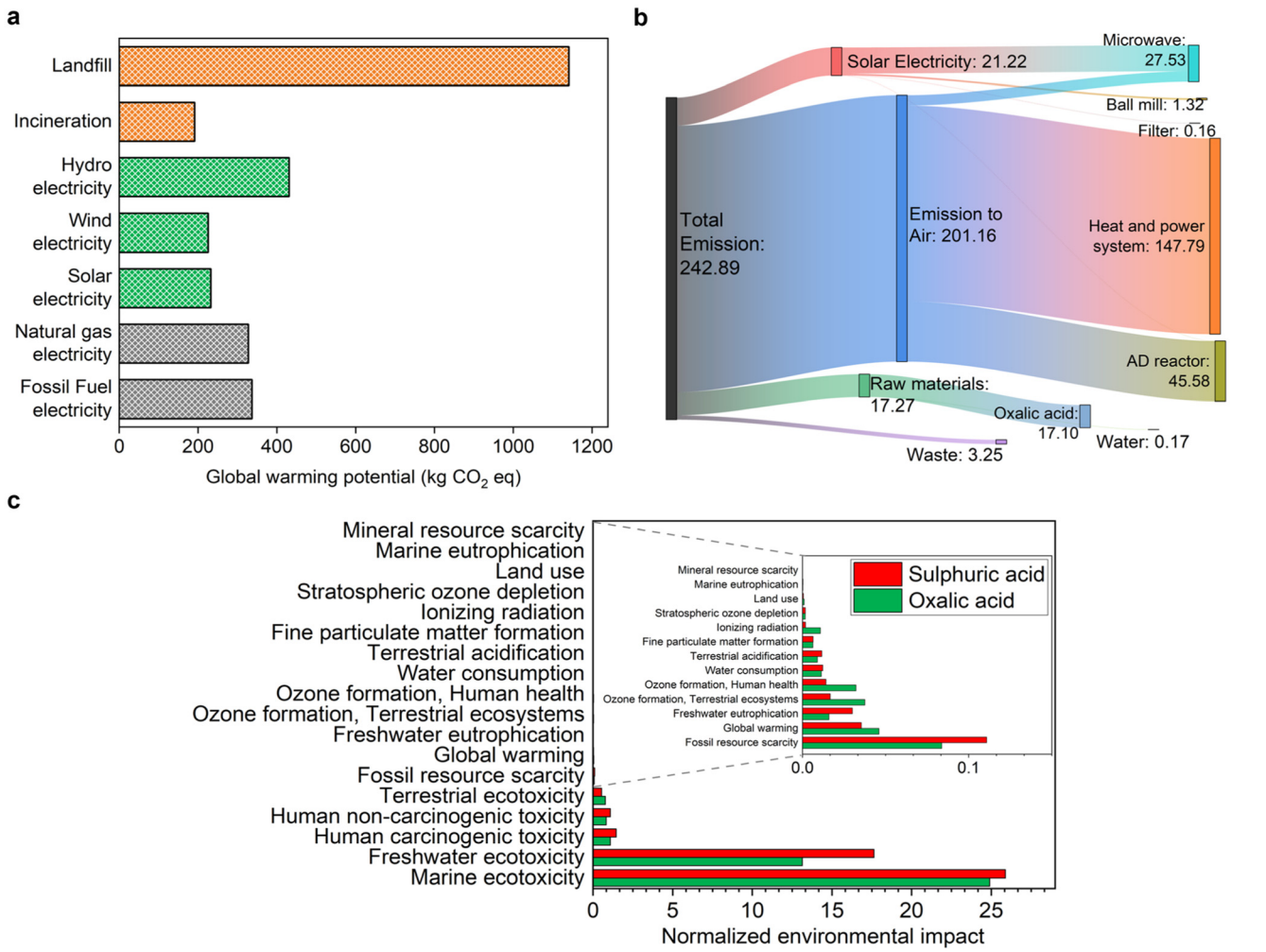

Fig. 5 Life cycle assessment of the CBW processes: (a) GWP of the mechano-bio-thermochemical (MBTC) and conventional management processes (incineration and landfill). Electricity from renewable sources (hydro, wind, solar), natural gas and fossil fuel were considered in the CBW MBTC process. (b) Sankey diagram of our CBW process driven by solar electricity. (c) Normalized environmental impact score evaluation of sulphuric acid and oxalic acid when used in the CBW MBTC process.

with photovoltaics generates biogas with low carbon emissions, at 95.1 kg CO_2 eq. This is particularly significant because it is independent of fossil fuels. Furthermore, integrating carbon capture and storage (CCS) into the CHP system could reduce the GWP associated with biogas combustion, as suggested by a previous study.[111]

Fig. 5c presents a normalized environmental impact score evaluation, revealing the comparative environmental performance of sulphuric and oxalic acids when integrated into our CBW process. Notably, OA exhibits a significant advantage over H_2SO_4 in terms of freshwater ecotoxicity. Although both acids show similarly high marine ecotoxicity scores (~25–26 points), OA has a slight edge. Furthermore, H_2SO_4 has slightly higher human toxicity scores for both non-carcinogenic and carcinogenic effects. An additional consideration is the dependence on fossil fuels, where H_2SO_4 production relies more heavily on fossil fuels compared to OA, highlighting OA's potential benefits in addressing fossil fuel scarcity. Overall, OA demonstrated a better environmental profile compared to H_2SO_4.

4. Conclusion

We developed an efficient green catalyst-enhanced mechano-chemical-microwave pretreatment approach for CBW to enhance sugar yield and biogas production. The optimized process involves co-milling CBW with green renewable solid oxalic acid, which offers several advantages over traditional mineral acid catalysts, such as sulfuric acid. OA co-milled CBW resulted in enhanced OA impregnation in CBW, reduced particle size, and increased surface area, in apparent contrast to milling without a catalyst. Efficient co-milling decreased the DP of cellulose, which increased the reducing ends, and transformed crystalline cellulose into more reactive amorphous cellulose through esterification of the C6–OH group, which disrupted intra- and intermolecular hydrogen bonds. Consequently, the cellulose structure became more reactive and accessible to subsequent microwave hydrothermal treatment, which facilitated the cleavage of β-1,4 glycosidic bonds. This released glucose products through OA deprotonation and hydronium ion formation, which ultimately yielded a remarkable sugar yield of 52.32 g per 100 g dried CBW, outperforming other acids. After MHT optimization, the production of sugar-degraded by-products, such as furfural and 5-HMF, was minimized with only 5 min of reaction time, maximizing the total sugar yield with 70% glucose yield and 100% xylose yield at 180 °C and 140 °C, respectively. This approach offers a simplified and energy-efficient process, achieving sugar extraction approximately 18.5 times faster than enzymatic hydrolysis. The pretreated CBW-OA feed, without sugar separation, exhibited great potential for biogas production, with an enhanced initial methane yield, making it a promising feedstock for anaerobic digestion and biogas production. LCA study reveals that the environmental benefits of this process are further enhanced when considering biogas production and the potential displacement of fossil fuels. Our study paves the way for more sustainable and cost-effective biofuel production from lignocellulosic waste materials.

Author contributions

Li Quan Lee and Hong Li conceived the ideas. Li Quan Lee and Hui Ling Chan developed the methodology, conducted investigations, performed comprehensive characterization analyses, curated the data, and authored the original draft. Hao Zhou conducted the life cycle analysis. Hu Zhao performed FE-SEM and XRD characterizations and provided resources, while Qingshuo Ao, Hao Huang and Chi Cheng Chong conducted HPLC, GPC and FTIR characterizations, respectively. Hong Li and Yan Zhou supervised the project, validated the results, and contributed to the review of manuscript and funding acquisition.

Data availability

The data supporting this article have been included as part of the ESI.†

Conflicts of interest

The authors declare no other competing interests.

Acknowledgements

This work was partially funded by the Agence Nationale de la Recherche (ANR) in the PEECFUEL project (ANR-23-CE05-0026). We would also like to acknowledge support from Conny Tech Pte Ltd, and Ms Lam Mei Shan from the NEWRI Analytics Cluster, Nanyang Technological University, Singapore, for her expertise on operating the HPLC for product characterization.

References

1 Y. Lu, T.-K. Liu, C. Lin, K. H. Kim, E. Kim, Y. Yang, *et al.*, Nanoconfinement Enables Photoelectrochemical Selective Oxidation of Glycerol via the Microscale Fluid Effect, *Nano Lett.*, 2024, **24**(15), 4633–4640.
2 Z.-H. Zhang, Z.-R. Yu, Y. Zhang, A. Barras, A. Addad, P. Roussel, *et al.*, Seawater corrosive engineering assisted *in situ* room temperature synthesis of Ni/Co/Fe trimetallic composition to achieve polyester plastics upgrading and green hydrogen production, *Chem. Eng. J.*, 2024, 155472.
3 J. K. Lee, J. H. Seo, J. Lim, S. Park and H. W. Jang, Best Practices in Membrane Electrode Assembly for Water Electrolysis, *ACS Mater. Lett.*, 2024, **6**, 2757–2786.

4 H. Wu, A. Singh-Morgan, K. Qi, Z. Zeng, V. Mougel and D. Voiry, Electrocatalyst microenvironment engineering for enhanced product selectivity in carbon dioxide and nitrogen reduction reactions, *ACS Catal.*, 2023, **13**(8), 5375–5396.
5 Z. Feng, R. Zhu, F. Chen, Y. Zhu, Y. Zhou, P. Guan, *et al.*, Recent advances in water-induced electricity generation based on 2D materials: A review, *J. Mater. Res.*, 2023, **38**(7), 1757–1779.
6 I. U. Khan, M. H. D. Othman, H. Hashim, T. Matsuura, A. Ismail, M. Rezaei-DashtArzhandi, *et al.*, Biogas as a renewable energy fuel–A review of biogas upgrading, utilisation and storage, *Energy Convers. Manage.*, 2017, **150**, 277–294.
7 J. Lyytimäki, Renewable energy in the news: Environmental, economic, policy and technology discussion of biogas, *Sustainable Prod. Consumption*, 2018, **15**, 65–73.
8 P. Kang, G. Song, M. Xu, T. R. Miller, H. Wang, H. Zhang, *et al.*, Low-carbon pathways for the booming express delivery sector in China, *Nat. Commun.*, 2021, **12**(1), 450.
9 N. Singapore, *Waste statistics and overall recycling*, Singapore National Environment Agency, 2022.
10 P. Kerdlap, J. S. C. Low and S. Ramakrishna, Zero waste manufacturing: A framework and review of technology, research, and implementation barriers for enabling a circular economy transition in Singapore, *Resour., Conserv. Recycl.*, 2019, **151**, 104438.
11 D. H. Vynios, D. A. Papaioannou, G. Filos, G. Karigiannis, T. Tziala and G. Lagios, Enzymatic production of glucose from waste paper, *BioResources*, 2009, **4**(2), 509–521.
12 H. Chen, R. A. Venditti, H. Jameel and S. Park, Enzymatic hydrolysis of recovered office printing paper with low enzyme dosages to produce fermentable sugars, *Appl. Biochem. Biotechnol.*, 2012, **166**, 1121–1136.
13 K. H. Chu and X. Feng, Enzymatic conversion of newspaper and office paper to fermentable sugars, *Process Saf. Environ. Prot.*, 2013, **91**(1–2), 123–130.
14 E. Dijkgraaf and H. R. Vollebergh, Burn or bury? A social cost comparison of final waste disposal methods, *Ecol. Econ.*, 2004, **50**(3–4), 233–247.
15 M. C. Monte, E. Fuente, A. Blanco and C. Negro, Waste management from pulp and paper production in the European Union, *Waste Manage.*, 2009, **29**(1), 293–308.
16 F. Sotoudehnia, A. B. Rabiu, A. Alayat and A. G. McDonald, Characterization of bio-oil and biochar from pyrolysis of waste corrugated cardboard, *J. Anal. Appl. Pyrolysis*, 2020, **145**, 104722.
17 L. Sørum, M. Grønli and J. Hustad, Pyrolysis characteristics and kinetics of municipal solid wastes, *Fuel*, 2001, **80**(9), 1217–1227.
18 A. Ahmad, M. Adil, A. Khalil and M. Rahman, Mechanical properties and durability of boardcrete blocks prepared from recycled cardboard, *J. Build. Eng.*, 2021, **33**, 101644.
19 J. Schönwälder and J. Rots, Cardboard: An innovative construction material, in *Sustainable Construction Materials and Technologies*, CRC Press, 2020, pp. 731–740.
20 Z. Kádár, Z. Szengyel and K. Réczey, Simultaneous saccharification and fermentation (SSF) of industrial wastes for the production of ethanol, *Ind. Crops Prod.*, 2004, **20**(1), 103–110.
21 X. Yuan, Y. Cao, J. Li, B. Wen, W. Zhu, X. Wang, *et al.*, Effect of pretreatment by a microbial consortium on methane production of waste paper and cardboard, *Bioresour. Technol.*, 2012, **118**, 281–288.
22 K. Pena Contreras, J. M. Sanchez Yanez, Q. Aguilar-Virgen, P. Taboada-González and L. Marquez-Benavides, Potential for methane generation by lignocellulosic household waste, *Sustainability*, 2018, **10**(10), 3461.
23 X. Fonoll, S. Astals, J. Dosta and J. Mata-Alvarez, Impact of paper and cardboard suppression on OFMSW anaerobic digestion, *Waste Manage.*, 2016, **56**, 100–105.
24 T. Kinnarinen and A. Häkkinen, Influence of enzyme loading on enzymatic hydrolysis of cardboard waste and size distribution of the resulting fiber residue, *Bioresour. Technol.*, 2014, **159**, 136–142.
25 R. Yáñez, J. Alonso and J. Parajó, Production of hemicellulosic sugars and glucose from residual corrugated cardboard, *Process Biochem.*, 2004, **39**(11), 1543–1551.
26 M. S. Jahan, M. M. Rahman and M. Sarkar, Upgrading old corrugated cardboard (OCC) to dissolving pulp, *Cellulose*, 2016, **23**, 2039–2047.
27 C. Chen, Y. Kuang, S. Zhu, I. Burgert, T. Keplinger, A. Gong, *et al.*, Structure–property–function relationships of natural and engineered wood, *Nat. Rev. Mater.*, 2020, **5**(9), 642–666.
28 Y. Hamzeh, S. Sabbaghi, A. Ashori, A. Abdulkhani and F. Soltani, Improving wet and dry strength properties of recycled old corrugated carton (OCC) pulp using various polymers, *Carbohydr. Polym.*, 2013, **94**(1), 577–583.
29 S. Pavlostathis, Giraldo–Gomez E. Kinetics of anaerobic treatment: a critical review, *Crit. Rev. Environ. Sci. Technol.*, 1991, **21**(5–6), 411–490.
30 N. Srivastava, R. Singh, P. Singh, I. Ahmad, R. P. Singh, A. K. Rai, *et al.*, Recent advances on lignocellulosic bioresources and their valorization in biofuels production: Challenges and viability assessment, *Environ. Technol. Innovation*, 2023, **29**, 103037.
31 Y. Sun and J. Cheng, Hydrolysis of lignocellulosic materials for ethanol production: a review, *Bioresour. Technol.*, 2002, **83**(1), 1–11.
32 T. Kinnarinen, M. Huhtanen, A. Häkkinen and M. Louhi-Kultanen, Solid–liquid separation of hydrolysates obtained from enzymatic hydrolysis of cardboard waste, *Ind. Crops Prod.*, 2012, **38**, 72–80.
33 L. P. Meleiro, A. L. R. L. Zimbardi, F. H. M. Souza, D. C. Masui, T. M. Silva, J. A. Jorge, *et al.*, A novel β-glucosidase from Humicola insolens with high potential for untreated waste paper conversion to sugars, *Appl. Biochem. Biotechnol.*, 2014, **173**, 391–408.
34 Ž Zebec, M. Poberžnik and A. Lobnik, Enzymatic hydrolysis of textile and cardboard waste as a glucose source for

the production of limonene in Escherichia coli, *Life*, 2022, **12**(9), 1423.
35 I. C. Hoeger, S. S. Nair, A. J. Ragauskas, Y. Deng, O. J. Rojas and J. Zhu, Mechanical deconstruction of lignocellulose cell walls and their enzymatic saccharification, *Cellulose*, 2013, **20**, 807–818.
36 A.-I. Yeh, Y.-C. Huang and S. H. Chen, Effect of particle size on the rate of enzymatic hydrolysis of cellulose, *Carbohydr. Polym.*, 2010, **79**(1), 192–199.
37 A. Teghammar, J. Yngvesson, M. Lundin, M. J. Taherzadeh and I. S. Horváth, Pretreatment of paper tube residuals for improved biogas production, *Bioresour. Technol.*, 2010, **101**(4), 1206–1212.
38 R. Zhang and Z. Zhu, Microwave assisted hydrothermal conversion of waste cardboard, *Process Saf. Environ. Prot.*, 2021, **156**, 209–218.
39 E. H. Koupaie, S. Dahadha, A. B. Lakeh, A. Azizi and E. Elbeshbishy, Enzymatic pretreatment of lignocellulosic biomass for enhanced biomethane production-A review, *J. Environ. Manage.*, 2019, **233**, 774–784.
40 Y. Li, S. Y. Park and J. Zhu, Solid-state anaerobic digestion for methane production from organic waste, *Renewable Sustainable Energy Rev.*, 2011, **15**(1), 821–826.
41 X. Tong and P. L. McCarty, Microbial hydrolysis of lignocellulosic materials, in *Methane from community wastes*, CRC Press, 1991, pp. 71–110.
42 S.-J. Yang, I. Kataeva, S. D. Hamilton-Brehm, N. L. Engle, T. J. Tschaplinski, C. Doeppke, *et al.*, Efficient degradation of lignocellulosic plant biomass, without pretreatment, by the thermophilic anaerobe "Anaerocellum thermophilum" DSM 6725, *Appl. Environ. Microbiol.*, 2009, **75**(14), 4762–4769.
43 H. L. Chan, H. Xu and Y. Zhou, External ceramic membrane contactor for *in situ* H2 assisted biogas upgrading, *Bioresour. Technol.*, 2024, 130981.
44 S. Sabiha-Hanim and N. A. Abd Halim, Sugarcane bagasse pretreatment methods for ethanol production, in *Fuel ethanol production from sugarcane*, 2018, pp. 63–79.
45 A. Ferrer, A. Requejo, A. Rodríguez and L. Jiménez, Influence of temperature, time, liquid/solid ratio and sulfuric acid concentration on the hydrolysis of palm empty fruit bunches, *Bioresour. Technol.*, 2013, **129**, 506–511.
46 S. C. Yat, A. Berger and D. R. Shonnard, Kinetic characterization for dilute sulfuric acid hydrolysis of timber varieties and switchgrass, *Bioresour. Technol.*, 2008, **99**(9), 3855–3863.
47 L. Q. Lee, H. Zhao, T. Y. Lim, G. Junyu, O. L. Ding, W. Liu, *et al.*, Green hydrogen generation assisted by electroreforming of raw sugarcane bagasse waste, *Green Chem.*, 2023, **25**(19), 7707–7720.
48 B.-Y. Cai, J.-P. Ge, H.-Z. Ling, K.-K. Cheng and W.-X. Ping, Statistical optimization of dilute sulfuric acid pretreatment of corncob for xylose recovery and ethanol production, *Biomass Bioenergy*, 2012, **36**, 250–257.
49 Y. Yan, C. Zhang, Q. Lin, X. Wang, B. Cheng, H. Li, *et al.*, Microwave-assisted oxalic acid pretreatment for the enhancing of enzyme hydrolysis in the production of xylose and arabinose from bagasse, *Molecules*, 2018, **23**(4), 862.
50 W. J. Sagues, J. Yang, N. Monroe, S.-D. Han, T. Vinzant, M. Yung, *et al.*, A simple method for producing bio-based anode materials for lithium-ion batteries, *Green Chem.*, 2020, **22**(20), 7093–7108.
51 A. M. J. Kootstra, H. H. Beeftink, E. L. Scott and J. P. Sanders, Comparison of dilute mineral and organic acid pretreatment for enzymatic hydrolysis of wheat straw, *Biochem. Eng. J.*, 2009, **46**(2), 126–131.
52 M. Maslin, L. Van Heerde and S. Day, Sulfur: A potential resource crisis that could stifle green technology and threaten food security as the world decarbonises, *Geogr. J.*, 2022, **188**(4), 498–505.
53 T. Shui, S. Feng, Z. Yuan, T. Kuboki and C. C. Xu, Highly efficient organosolv fractionation of cornstalk into cellulose and lignin in organic acids, *Bioresour. Technol.*, 2016, **218**, 953–961.
54 T. Zhang, R. Kumar and C. E. Wyman, Sugar yields from dilute oxalic acid pretreatment of maple wood compared to those with other dilute acids and hot water, *Carbohydr. Polym.*, 2013, **92**(1), 334–344.
55 H.-Y. Kim, J.-W. Lee, T. W. Jeffries and I.-G. Choi, Response surface optimization of oxalic acid pretreatment of yellow poplar (Liriodendron tulipifera) for production of glucose and xylose monosaccarides, *Bioresour. Technol.*, 2011, **102**(2), 1440–1446.
56 P. Hu, Y. Zhang, J. Huang, T. Liu, Y. Yuan and N. Xue, Eco-friendly leaching and separation of vanadium over iron impurity from vanadium-bearing shale using oxalic acid as a leachant, *ACS Sustainable Chem. Eng.*, 2018, **6**(2), 1900–1908.
57 S. H. Anita, F. Fitria, N. N. Solihat, F. P. Sari, L. Risanto, W. Fatriasari, *et al.*, Optimization of microwave-assisted oxalic acid pretreatment of oil palm empty fruit bunch for production of fermentable sugars, *Waste Biomass Valorization*, 2020, **11**, 2673–2687.
58 B. Cheng, X. Zhang, Q. Lin, F. Xin, R. Sun, X. Wang, *et al.*, A new approach to recycle oxalic acid during lignocellulose pretreatment for xylose production, *Biotechnol. Biofuels*, 2018, **11**, 1–9.
59 T. M. Lacerda, M. D. Zambon and E. Frollini, Oxalic acid as a catalyst for the hydrolysis of sisal pulp, *Ind. Crops Prod.*, 2015, **71**, 163–172.
60 *Oxalic Acid Pretreatment on Enhancement of Enzymatic Saccharification from Napier Grass for Biofuel Production*, ed. D. Panyarachun, E. J. Panakkal, A. Tawai, W. Rodiahwati, B. Paramasivam and S. Asavasanti, *et al.*, E3S Web of Conferences, EDP Sciences, 2023.
61 S.-Y. Jeong, B. Koo and J.-W. Lee, Structural changes in biomass (yellow poplar and empty fruit bunch) during hydrothermal and oxalic acid pretreatments and their effects on enzymatic hydrolysis efficiency, *Ind. Crops Prod.*, 2022, **178**, 114569.

62 B. Szczęśniak, S. Borysiuk, J. Choma and M. Jaroniec, Mechanochemical synthesis of highly porous materials, *Mater. Horiz.*, 2020, **7**(6), 1457–1473.
63 S. Głowniak, B. Szczęśniak, J. Choma and M. Jaroniec, Mechanochemistry: Toward green synthesis of metal–organic frameworks, *Mater. Today*, 2021, **46**, 109–124.
64 E. C. Gaudino, G. Cravotto, M. Manzoli and S. Tabasso, Sono-and mechanochemical technologies in the catalytic conversion of biomass, *Chem. Soc. Rev.*, 2021, **50**(3), 1785–1812.
65 Q. Lu, W. Lin, L. Tang, S. Wang, X. Chen and B. Huang, A mechanochemical approach to manufacturing bamboo cellulose nanocrystals, *J. Mater. Sci.*, 2015, **50**, 611–619.
66 W. Zhang, M. Liang and C. Lu, Morphological and structural development of hardwood cellulose during mechanochemical pretreatment in solid state through pan-milling, *Cellulose*, 2007, **14**, 447–456.
67 G. Pablo, B. Gullón, A. Romaní and G. Garrote, Fast-growing Paulownia wood fractionation by microwave-assisted hydrothermal treatment: A kinetic assessment, *Bioresour. Technol.*, 2021, **338**, 125535.
68 G. Pablo, A. Pérez-Pérez, G. Garrote and B. Gullón, Manufacturing of hemicellulosic oligosaccharides from fast-growing Paulownia wood via autohydrolysis: Microwave versus conventional heating, *Ind. Crops Prod.*, 2022, **187**, 115313.
69 J. Feng, J. Jiang, C.-Y. Hse, Z. Yang, K. Wang, J. Ye, *et al.*, Selective catalytic conversion of waste lignocellulosic biomass for renewable value-added chemicals via directional microwave-assisted liquefaction, *Sustainable Energy Fuels*, 2018, **2**(5), 1035–1047.
70 Z. Zhu, C. A. Rezende, R. Simister, S. J. McQueen-Mason, D. J. Macquarrie, I. Polikarpov, *et al.*, Efficient sugar production from sugarcane bagasse by microwave assisted acid and alkali pretreatment, *Biomass Bioenergy*, 2016, **93**, 269–278.
71 Z. Zhu, Y. Liu, L. D. Gómez, T. Wei, X. Yang, R. Simister, *et al.*, Thermochemical pretreatments of maize stem for sugar recovery: Comparative evaluation of microwave and conventional heating, *Ind. Crops Prod.*, 2021, **160**, 113106.
72 L. Q. Lee, H. Zhao, J. Ge, Y. Zhou and H. Li, Valorization of fast-growing Paulownia wood to green chemicals and green hydrogen, *Green Chem.*, 2024, **26**(4), 1949–1963.
73 A. Sluiter, R. Ruiz, C. Scarlata, J. Sluiter and D. Templeton, Determination of extractives in biomass, *Lab. Anal. Proced.*, 2005, **1617**(4), 1–16.
74 C. S. Eskilsson and E. Björklund, Analytical-scale microwave-assisted extraction, *J. Chromatogr., A*, 2000, **902**(1), 227–250.
75 A. Sluiter, B. Hames, R. Ruiz, C. Scarlata, J. Sluiter, D. Templeton, *et al.*, Determination of structural carbohydrates and lignin in biomass, *Lab. Anal. Proced.*, 2008, **1617**(1), 1–16.
76 A. Sluiter, J. Sluiter and E. J. Wolfrum, Methods for biomass compositional analysis, in *Catalysis for the conversion of biomass and its derivatives*, 2013, p. 2.
77 S. Y. Oh, D. I. Yoo, Y. Shin, H. C. Kim, H. Y. Kim, Y. S. Chung, *et al.*, Crystalline structure analysis of cellulose treated with sodium hydroxide and carbon dioxide by means of X-ray diffraction and FTIR spectroscopy, *Carbohydr. Res.*, 2005, **340**(15), 2376–2391.
78 X. Sun, R. Sun, P. Fowler and M. Baird, Isolation and characterisation of cellulose obtained by a two-stage treatment with organosolv and cyanamide activated hydrogen peroxide from wheat straw, *Carbohydr. Polym.*, 2004, **55**(4), 379–391.
79 R. Cohen, K. A. Jensen, C. J. Houtman and K. E. Hammel, Significant levels of extracellular reactive oxygen species produced by brown rot basidiomycetes on cellulose, *FEBS Lett.*, 2002, **531**(3), 483–488.
80 A. Mittal, R. Katahira, M. E. Himmel and D. K. Johnson, Effects of alkaline or liquid-ammonia treatment on crystalline cellulose: changes in crystalline structure and effects on enzymatic digestibility, *Biotechnol. Biofuels*, 2011, **4**, 1–16.
81 Z. Zhou, Y. Wang, M. Wang and Z. Zhou, Co-metabolic Effect of Glucose on Methane Production and Phenanthrene Removal in an Enriched Phenanthrene-Degrading Consortium Under Methanogenesis, *Front. Microbiol.*, 2021, **12**, 749967.
82 A. Ware and N. Power, Modelling methane production kinetics of complex poultry slaughterhouse wastes using sigmoidal growth functions, *Renewable Energy*, 2017, **104**, 50–59.
83 ISO I. 14040, *Environmental management—life cycle assessment—principles and framework*, 2006, pp. 235–248.
84 M. Finkbeiner, A. Inaba, R. Tan, K. Christiansen and H.-J. Klüppel, The new international standards for life cycle assessment: ISO 14040 and ISO 14044, *Int. J. Life Cycle Assess.*, 2006, **11**, 80–85.
85 ed. V. S. Chang, B. Burr and M. T. Holtzapple, Lime pretreatment of switchgrass. Biotechnology for Fuels and Chemicals: Proceedings of the Eighteenth Symposium on Biotechnology for Fuels and Chemicals Held May 5–9, 1996, at Gatlinburg, Tennessee, Springer, 1997.
86 A. W. Tricker, G. Samaras, K. L. Hebisch, M. J. Realff and C. Sievers, Hot spot generation, reactivity, and decay in mechanochemical reactors, *Chem. Eng. J.*, 2020, **382**, 122954.
87 A. Barakat, C. Mayer-Laigle, A. Solhy, R. A. Arancon, H. De Vries and R. Luque, Mechanical pretreatments of lignocellulosic biomass: towards facile and environmentally sound technologies for biofuels production, *RSC Adv.*, 2014, **4**(89), 48109–48127.
88 E. Dengiz Özcan, K. Çinku, Ş. Özdamar, H. Ergin and Ş. G Özkan, Investigation of the effect of polymer-based novel grinding aids on cement grinding efficiency, *J. Appl. Polym. Sci.*, 2022, **139**(13), 51870.
89 H. Choi, W. Lee and S. Kim, Effect of grinding aids on the kinetics of fine grinding energy consumed of calcite powders by a stirred ball mill, *Adv. Powder Technol.*, 2009, **20**(4), 350–354.

90 N. Terinte, R. Ibbett and K. C. Schuster, Overview on native cellulose and microcrystalline cellulose I structure studied by X-ray diffraction (WAXD): Comparison between measurement techniques, *Lenzinger Ber.*, 2011, **89**(1), 118–131.
91 G. Tofani, I. Cornet and S. Tavernier, Separation and recovery of lignin and hydrocarbon derivatives from cardboard, *Biomass Convers. Biorefin.*, 2022, 1–16.
92 J. L. Perez-Rodriguez, A. Durán, M. Centeno, J. M. Martínez-Blanes and M. Robador, Thermal analysis of monument patina containing hydrated calcium oxalates, *Thermochim. Acta*, 2011, **512**(1–2), 5–12.
93 H. Xu, L. Huang, M. Xu, M. Qi, T. Yi, Q. Mo, *et al.*, Preparation and properties of cellulose-based films regenerated from waste corrugated cardboards using [Amim]Cl/$CaCl_2$, *ACS Omega*, 2020, **5**(37), 23743–23754.
94 D. Ciolacu, F. Ciolacu and V. I. Popa, Amorphous cellulose—structure and characterization, *Cellul. Chem. Technol.*, 2011, **45**(1), 13.
95 J. Henschen, D. Li and M. Ek, Preparation of cellulose nanomaterials via cellulose oxalates, *Carbohydr. Polym.*, 2019, **213**, 208–216.
96 M. Tyufekchiev, A. Kolodziejczak, P. Duan, M. Foston, K. Schmidt-Rohr and M. T. Timko, Reaction engineering implications of cellulose crystallinity and water-promoted recrystallization, *Green Chem.*, 2019, **21**(20), 5541–5555.
97 N. S. Mosier, A. Sarikaya, C. M. Ladisch and M. R. Ladisch, Characterization of dicarboxylic acids for cellulose hydrolysis, *Biotechnol. Prog.*, 2001, **17**(3), 474–480.
98 V. Kumar, M. Irfan and A. Datta, Manipulation of oxalate metabolism in plants for improving food quality and productivity, *Phytochemistry*, 2019, **158**, 103–109.
99 T. Runge and C. Zhang, Two-stage acid-catalyzed conversion of carbohydrates into levulinic acid, *Ind. Eng. Chem. Res.*, 2012, **51**(8), 3265–3270.
100 E. Schuler, L. Grooten, M. Kasireddy, S. More, N. R. Shiju, S. K. Tanielyan, *et al.*, Oxalic acid hydrogenation to glycolic acid: heterogeneous catalysts screening, *Green Chem.*, 2023, **25**(6), 2409–2426.
101 J. Zhu and X. Pan, Efficient sugar production from plant biomass: Current status, challenges, and future directions, *Renewable Sustainable Energy Rev.*, 2022, **164**, 112583.
102 J.-L. Wertz, J. P. Mercier and O. Bédué, *Cellulose science and technology*, CRC Press, 2010.
103 P. Sannigrahi, D. H. Kim, S. Jung and A. Ragauskas, Pseudo-lignin and pretreatment chemistry, *Energy Environ. Sci.*, 2011, **4**(4), 1306–1310.
104 G. D. Brown, J. Bauer, H. M. Osborn and R. Kuemmerle, A solution NMR approach to determine the chemical structures of carbohydrates using the hydroxyl groups as starting points, *ACS Omega*, 2018, **3**(12), 17957–17975.
105 K. Liew, A. Sojobi and L. Zhang, Green concrete: Prospects and challenges, *Constr. Build. Mater.*, 2017, **156**, 1063–1095.
106 P. Jędrzejczak, M. N. Collins, T. Jesionowski and Ł. Klapiszewski, The role of lignin and lignin-based materials in sustainable construction–a comprehensive review, *Int. J. Biol. Macromol.*, 2021, **187**, 624–650.
107 S. B. Jilani and D. G. Olson, Mechanism of furfural toxicity and metabolic strategies to engineer tolerance in microbial strains, *Microb. Cell Fact.*, 2023, **22**(1), 221.
108 A. Cohen, R. Zoetemeyer, A. Van Deursen and J. Van Andel, Anaerobic digestion of glucose with separated acid production and methane formation, *Water Res.*, 1979, **13**(7), 571–580.
109 A. Wang, P. Shao, F. Lan and H. Jin, Organic chemicals in coal available to microbes to produce biogenic coalbed methane: A review of current knowledge, *J. Nat. Gas Sci. Eng.*, 2018, **60**, 40–48.
110 W. Li, H. Khalid, Z. Zhu, R. Zhang, G. Liu, C. Chen, *et al.*, Methane production through anaerobic digestion: Participation and digestion characteristics of cellulose, hemicellulose and lignin, *Appl. Energy*, 2018, **226**, 1219–1228.
111 Y. Ma, H. Wang, F. Hong, J. Yang, Z. Chen, H. Cui, *et al.*, Modeling and optimization of combined heat and power with power-to-gas and carbon capture system in integrated energy system, *Energy*, 2021, **236**, 121392.